Spectroscopic Investigation of Reduced Protocatechuate 3,4-Dioxygenase: Charge-Induced Alterations in the Active Site Iron Coordination Environment

Mindy I. Davis,[†] Erik C. Wasinger,[†] Tami E. Westre,[†] Jeffrey M. Zaleski,[†] Allen M. Orville,[§] John D. Lipscomb,*[,§] Britt Hedman,*[,†,‡] Keith O. Hodgson,*[,†,‡] and Edward I. Solomon*[,†]

Department of Chemistry and Stanford Synchrotron Radiation Laboratory, Stanford University, Stanford, California 94305, and Department of Biochemistry and the Center for Metals in Biocatalysis, University of Minnesota, Minneapolis, Minnesota 55455

Received December 22, 1998

Chemical reduction of the mononuclear ferric active site in the bacterial intradiol cleaving catecholic dioxygenase protocatechuate 3,4-dioxygenase (3,4-PCD, *Brevibacterium fuscum*) produces a high-spin ferrous center. We have applied circular dichroism (CD), magnetic circular dichroism (MCD), variable-temperature-variable-field (VTVH) MCD, X-ray absorption (XAS) pre-edge, and extended X-ray absorption fine structure (EXAFS) spectroscopies to investigate the geometric and electronic structure of the reduced iron center. Excited-state ligand field CD and MCD data indicate that the site is six-coordinate where the ^5E_g excited-state splitting is 2033 cm^{-1}. VTVH MCD analysis of the ground state indicates that the site has negative zero-field splitting with a small rhombic splitting of the lowest doublet ($\delta = 1.6 \pm 0.3$ cm^{-1}). XAS pre-edge analysis also indicates a six-coordinate site while EXAFS analysis provides accurate bond lengths. Since previous spectroscopic analysis and the crystal structure of oxidized 3,4-PCD indicate a five-coordinate ferric active site, the results presented here show that the coordination number increases upon reduction. This is attributed to the coordination of a second solvent ligand. The coordination number increase relative to the oxidized site also appears to be associated with a large decrease in the ligand donor strength in the reduced enzyme due to protonation of the original hydroxide ligand.

Introduction

Mononuclear non-heme iron active sites are present in a variety of protein systems that perform important biological functions involving dioxygen.[1−4] One such class of enzymes, the bacterial catecholic dioxygenases, catalyzes the cleavage of molecular oxygen with concomitant insertion of both oxygen atoms into the aromatic ring of the substrate, resulting in ring cleavage. These enzymes are important in the degradation of natural products as well as xenobiotic pollutants.[2,5,6] This type of dioxygenase can be divided further into two broad classes termed intra- or extradiol, depending on the position of ring cleavage. The extradiol dioxygenases utilize Fe^{2+} (and in one enzyme Mn^{2+})[7] to specifically cleave the ring on one side or the other of the vicinal hydroxyl groups of the catecholic substrate, while the intradiol dioxygenases use Fe^{3+} to cleave between the hydroxylated carbon atoms of the ring.[2] This correlation of metal redox state with ring cleavage site, together with a number of studies indicating differences in the electronic and geometric structural characteristics of the metal centers and their interactions with substrates, has led to different proposals for the mechanism of each dioxygenase.[1,2] At the root of each of these proposals is the concept that the specific charge on the metal center leads to distinct enzyme−substrate complexes and consequently different interactions of the metal center with O_2 that result in different reaction outcomes.

Protocatechuate 3,4-dioxygenase (3,4-PCD, EC 1.13.11.3) is an intradiol cleaving catecholic dioxygenase that has been isolated from or identified in over a dozen bacterial species.[2] It catalyzes the cleavage of protocatechuic acid to *β*-carboxy-*cis*,-*cis*-muconate with the incorporation of both atoms of oxygen from molecular oxygen.[8] This is a key reaction in the degradation pathways of several, more complex, aromatic compounds.[2] 3,4-PCD is the most extensively studied intradiol dioxygenase. X-ray crystallographic structures are available for the enzyme isolated from *Pseudomonas putida*[9] (left side of Scheme 1) and its complexes with substrates, substrate analogues, inhibitors, and oxygen analogues.[10−14] The active site geometry of the resting ferric enzyme is distorted trigonal bipyramidal with

[†] Department of Chemistry, Stanford University.
[‡] Stanford Synchrotron Radiation Laboratory.
[§] University of Minnesota.

(1) Que, L., Jr.; Ho, R. Y. N. *Chem. Rev.* **1996**, *96*, 2607−2624.
(2) Lipscomb, J. D.; Orville, A. M. In *Degradation of Environmental Pollutants by Microorganisms and Their Metalloenzymes*; Sigel, H., Sigel, A., Eds.; Marcel Dekker: New York, 1992; *Metal Ions in Biological Systems* Vol. 28, pp 243−298.
(3) Feig, A. L.; Lippard, S. J. *Chem. Rev.* **1994**, *94*, 759−805.
(4) Hegg, E. L.; Que, L., Jr. *Eur. J. Biochem.* **1997**, *250*, 625−629.
(5) Dagley, S. In *The Bacteria*; Sokatch, J. R., Ornston, L. N., Eds.; Academic Press: Orlando, FL 1986; Vol. 10, Chapter 10, pp 527−555.
(6) Levin, M. A.; Gealt, M. A. In *Biotreatment of Industrial and Hazardous Waste*; Levin, M. A., Gealt, M. A., Eds.; McGraw-Hill: New York, 1993; pp 5−7.
(7) Boldt, Y. R.; Sadowsky, M. J.; Ellis, L. B. M.; Que, L., Jr.; Wackett, L. P. *J. Bacteriol.* **1995**, *177*, 1225−1232.
(8) Fujisawa, H.; Hayaishi, O. *J. Biol. Chem.* **1968**, *243*, 267−281.
(9) The CD spectra of 3,4-PCD isolated from *P. putida* and *B. fuscum* were identical in both the oxidized and the reduced forms. Therefore a comparison can be made between the studies here on *B. fuscum* 3,4-PCD and the crystallography on *P. putida* 3,4-PCD.
(10) Ohlendorf, D. H.; Orville, A. M.; Lipscomb, J. D. *J. Mol. Biol.* **1994**, *244*, 586−608.
(11) Elgren, T. E.; Orville, A. M.; Kelly, K. A.; Lipscomb, J. D.; Ohlendorf, D. H.; Que, L. Jr. *Biochemistry* **1997**, *36*, 11504−11513.

10.1021/ic981464p CCC: $18.00
Published on Web 07/15/1999

Scheme 1

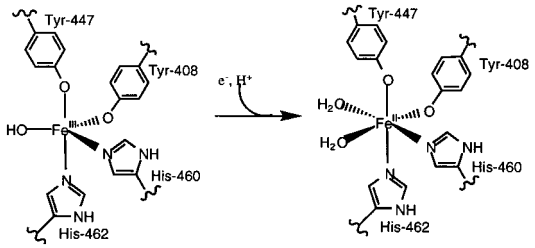

The numbering scheme used is from *P. putida*; *Ohlendorf et al.*[10]

histidine and tyrosine as axial ligands and histidine, hydroxide, and tyrosine as equatorial ligands.

Shifts in the ligation and coordination number appear to be integral to the function of 3,4-PCD. Spectroscopic and crystallographic studies have shown that catecholic substrate binding results in displacement of the hydroxide and the axial tyrosine ligands. The substrate binds asymmetrically with the longer iron−catecholate bond *trans* to Tyr408, and the coordination geometry shifts to square pyramidal with an open coordination position. This new open position can be occupied by small molecules such as CN^-.[13] We have speculated that this iron site may serve to bind the distal oxygen atom in the peroxy-substrate intermediate during catalysis, thereby facilitating O−O bond cleavage.[2,13] Similar changes in coordination number and geometry have been observed for the ferrous form of the enzyme after binding NO to convert the enzyme to an EPR-active form.[15,16] The spectroscopic analysis of these nitrosyl complexes involves a d^7 system comprised of a high-spin ferric site antiferromagnetically coupled to an $S = 1$ NO^- which has an $S = {}^3/_2$ ground state.[17] Using isotopically labeled aromatic ligands, it was shown that the catecholic substrate and NO can bind simultaneously to the iron, apparently resulting in the displacement of the solvent ligand. Addition of CN^- prior to NO in the absence of substrate yielded an unusual $S = {}^1/_2$ complex in which the coordination number apparently increased to six attendant with displacement of the axial tyrosine and the binding of at least two cyanides and NO to the iron.[16]

The nature of the iron ligation is influenced by the charge of the metal center in at least two ways. First, the charge on the ligand *trans* to the position of exogenous ligand binding appears to alter the strength of the bond that is formed. This effect is observed through the asymmetry of the iron(III)−catecholate bond lengths in the crystal structures and differences in hyperfine coupling of the two CN^- ligands in the iron(II)−nitrosyl complexes.[10,13,16] Second, the ligation of the metal center of 3,4-PCD appears to adapt to maintain a neutral net charge through protonation or ligand exchange, as indicated from spectroscopic and crystallographic analysis of the substrate complexes and the NO complexes. Similar factors appear to affect the complexes formed at the ferrous centers of the extradiol dioxygenases.[18−20]

Studies of the ferrous site allow one to examine specific changes that occur upon reduction of the metal center. If net charge is a determining factor in metal site structure, then we would expect changes in the ligation of 3,4-PCD to occur to compensate for the shift in the charge on the metal. Unfortunately, past efforts to probe the active site of the ferrous 3,4-PCD in the absence of the reactive NO ligand have provided limited information because the chromophore and EPR spectrum of the ferric center are lost upon reduction. Although analysis of Mössbauer data did indicate that the coordination number of 3,4-PCD changes upon reduction, it was fit well by either a distorted tetrahedral or an octahedral high-spin rhombic model. Thus it did not provide definitive information about the effect of the redox state of the iron on the nature of the metal ligation.[21,22]

In the current study, we have used circular dichroism (CD), low-temperature magnetic circular dichroism (MCD), variable-temperature−variable-field (VTVH) MCD, and X-ray absorption (XAS) edge and extended X-ray absorption fine structure (EXAFS) spectroscopies to study the geometric and electronic structure of the reduced form of 3,4-PCD in order to evaluate the effect of the charge of the active site metal on ligation sphere. CD and MCD spectroscopy in the near-IR region allows for the direct observation of d→d transitions to the ^5E_g excited state, which is split by the low symmetry of the protein active site. By using methodology developed for high spin, $S = 2$ Fe^{2+} systems,[23−25] the energy and splitting of these d→d transitions can be used to determine the coordination number, geometry, and, by comparison to model complexes, the nature of the ligands. For a high-spin ferrous system with an $S = 2$ ground state, the VTVH saturation magnetization MCD intensity isotherms do not superimpose when plotted as a function of $\beta H/2k_BT$ (β is the Bohr magneton and k_B is Boltzmann's constant). Analysis of the non-Kramers behavior can be used to obtain detailed insight into the $^5T_{2g}$ ferrous ground state. Additionally, analysis of the 1s→3d XAS pre-edge intensities and energy multiplet splittings provides complementary information on coordination number, oxidation state, and geometry,[26] while EXAFS provides accurate bond lengths and insight into the nature of the ligands. Together these methods provide detailed information on the electronic and geometric structure of reduced 3,4-PCD and therefore the change in the active site upon reduction. The data indicate that the change which occurs is consistent with previous proposals of an active site structure that responds to the net charge on the metal center. This serves as a basis for considering the origins of the different active site

(12) Frazee, R. W.; Orville, A. M.; Dolbeare, K. B.; Yu, H.; Ohlendorf, D. H.; Lipscomb, J. D. *Biochemistry* **1998**, *37*, 2131−2144.
(13) Orville, A. M.; Lipscomb, J. D.; Ohlendorf, D. H. *Biochemistry* **1997**, *36*, 10052−10066.
(14) Orville, A. M.; Elango, N.; Lipscomb, J. D.; Ohlendorf, D. H. *Biochemistry* **1997**, *36*, 10039−10051.
(15) Orville, A. M.; Lipscomb, J. D. *J. Biol. Chem.* **1993**, *268*, 8596−8607.
(16) Orville, A. M.; Lipscomb, J. D. *Biochemistry* **1997**, *36*, 14044−14055.
(17) Brown, C. A.; Pavlovsky, M. A.; Westre, T. E.; Zhang, Y.; Hedman, B.; Hodgson, K. O.; Solomon, E. I. *J. Am. Chem. Soc.* **1995**, *117*, 715−732.
(18) Han, S.; Eltis, L. D.; Timmis, K. N.; Muchmore, S. W.; Bolin, J. T. *Science* **1995**, *270*, 976−980.
(19) Shu, L.; Chiou, Y.-M.; Orville, A. M.; Miller, M. A.; Lipscomb, J. D.; Que, L., Jr. *Biochemistry* **1995**, *34*, 6649−6659.
(20) Senda, T.; Sugiyama, K.; Narita, H.; Yamamoto, T.; Kimbara, K.; Fukuda, M.; Sato, M.; Yano, K.; Mitsui, Y. *J. Mol. Biol.* **1996**, *255*, 735−752.
(21) Que, L., Jr.; Lipscomb, J. D.; Zimmermann, R.; Münck, E.; Orme-Johnson, N. R.; Orme-Johnson, W. H. *Biochim. Biophys. Acta* **1976**, *452*, 320−334.
(22) Zimmermann, R.; Huynh, B. H.; Münck, E.; Lipscomb, J. D. *J. Chem. Phys.* **1978**, *69*, 5463−5467.
(23) Pavel, E. G.; Kitajima, N.; Solomon, E. I. *J. Am. Chem. Soc.* **1998**, *120*, 3949−3962.
(24) Solomon, E. I.; Pavel, E. G.; Loeb, K. E.; Campochiaro, C. *Coord. Chem. Rev.* **1995**, *144*, 369−460.
(25) Whittaker, J. W.; Solomon, E. I. *J. Am. Chem. Soc.* **1988**, *110*, 5329−5339.
(26) Westre, T. E.; Kennepohl, P.; DeWitt, J. G.; Hedman, B.; Hodgson, K. O.; Solomon, E. I. *J. Am. Chem. Soc.* **1997**, *119*, 6297−6314.

structures and ring cleavage specificities of intradiol and extradiol enzymes.

Experimental Section

Sample Preparation. Protocatechuate 3,4-dioxygenase from *Brevibacterium fuscum* was purified as previously reported, stored at −80 °C, and thawed immediately prior to use.[27,28] All commercial reagents were of the highest grade available and were used without further purification. The ferric 3,4-PCD, in 50 mM MOPS buffer (3-[*N*-morpholino]propanesulfonic acid; pH = 7; Sigma), was rigorously degassed at 4 °C in a Teflon-stoppered flask by evacuating and filling with Ar 15 times, and then immediately placed in a dry N_2 atmosphere glovebox. Sodium dithionite (Sigma) was prepared just prior to use in Ar-purged deionized H_2O. A small aliquot of this solution (7-fold excess equiv) was added to 3,4-PCD (maintained at 4 °C) and allowed to react for up to 30 min while being thoroughly mixed. The reduction was complete when the color of the enzyme bleached from the characteristic red color (λ_{max} = 460 nm) to colorless.[15] When the solution was exposed to air or when potassium ferricyanide was added anaerobically, the red color reappeared, indicating that the reaction is reversible.[29] CD spectra with dithionite present were compared to those after the dithionite was anaerobically removed (by dilutions with MOPS buffer followed by concentration with a Centricon) and found to be unperturbed by the presence of dithionite. For the MCD and XAS experiments, 50% (v/v) glycerol, degassed under vacuum by freeze/pump/thaw/heat procedures, was added as a glassing agent. CD spectra were taken with and without glycerol to ensure that the protein was unaffected by the glassing agent. MOPS buffer prepared in D_2O (99.9 atom % D; Aldrich) and adjusted to a pD of 7.4 with NaOD (Aldrich), sodium dithionite dissolved in D_2O, and glycerol-d_3 (98 atom % D; Cambridge Isotopes Laboratories) were used to eliminate the hydroxide stretches which dominate the IR absorption spectrum above 1600 nm.

Circular Dichroism and Magnetic Circular Dichroism Measurements. The data were collected on a Jasco J-200D (600−2000 nm) spectropolarimeter interfaced to a Macintosh IIvx computer with LabVIEW software (National Instruments), and a liquid N_2-cooled InSb detector. The J-200D is equipped with an Oxford Instruments SM4000−7 T superconducting magnet/cryostat capable of fields up to 7.0 T and temperatures down to 1.5 K. CD samples (1.8−2.0 mM in iron) were prepared in a 1 cm path length anaerobic cuvette and were kept at 4 °C at all times with a circulating cooling bath attached to the sample holder. Contributions to the CD intensity due to buffer and cell backgrounds were subtracted from the raw protein CD spectra. Low-temperature (1.6−50.2 K) MCD spectra were obtained in a copper MCD sample cell with two Infrasil quartz disks sandwiching a 3 mm thick neoprene O-ring spacer through which the sample was injected. MCD samples were quick frozen in liquid N_2 immediately after preparation and were loaded into the cryostat under a high flow of helium gas. The depolarization of the frozen MCD sample, checked by measuring the CD spectrum of a nickel (+)-tartrate solution placed before and after the sample, was less than 5%.[30] The MCD spectra were corrected for the natural CD and zero-field baseline effects caused by strain in the glasses by subtracting the 0 T scan from each of the other field scans at a given temperature. The baseline-corrected CD and MCD spectra were fit to Gaussian band shapes using a modified Levenberg−Marquardt constrained nonlinear least-squares procedure. VTVH data were normalized to the maximum observed intensity and fit to an orientation-averaged intensity expression which includes rhombic and Zeeman splitting of a non-Kramers doublet, as well as the transition polarization ratio and contributions from linear temperature-independent B-terms and low-lying excited states.[23,24] Data were fit to both positive and negative zero-field splitting (ZFS) models to determine the best fit as discussed elsewhere.[31]

X-ray Absorption Measurements. XAS samples (3 mM in iron) were transferred into a Lucite XAS cell with 37 μm Kapton windows, and frozen in liquid nitrogen. The EPR spectrum of the sample was taken to ensure absence of a ferric signal. X-ray absorption spectra were recorded at the Stanford Synchrotron Radiation Laboratory (SSRL) on unfocused beamline 7−3 during ring conditions of 3 GeV and 50−100 mA. Monochromatism of the radiation was achieved using a Si(220) double-crystal monochromator. Data were measured to k = 15 Å^{-1} with 1 mm vertical pre-monochromator beam defining slits, and the monochromator was detuned to 50% at 7998 eV to minimize harmonic contamination. An Oxford Instruments continuous-flow liquid helium CF1208 cryostat was used to maintain a constant sample temperature of 10 K. Energies were calibrated using an internal Fe foil standard, assigning the first inflection point to 7111.2 eV.[32] The spectrometer energy resolution was ~1.4 eV with a reproducibility in the edge position of <0.2 eV. The fluorescence signal was monitored using a 13-element Ge solid-state array detector electronically windowed on the Fe Kα signal.[33]

EXAFS data reduction was performed on the normalized protein spectra according to established methods.[34−36] A smooth pre-edge background was removed from the averaged spectra by fitting a Gaussian polynomial to the pre-edge region and subtracting this polynomial from the entire spectrum, and the normalized data were converted to k-space. The photoelectron wave vector, k, is defined by $[2m_e(E - E_o)\hbar^2]^{1/2}$, where m_e is the electron mass, E is the photon energy, h is Planck's constant divided by 2π, and E_o is the threshold energy of the absorption edge, which was defined to be 7130 eV for the Fe K absorption edge. A spline through the EXAFS region was chosen so that it minimized residual low-frequency background but did not reduce the EXAFS amplitude as checked by monitoring the Fourier transform of the EXAFS during the background subtraction process.

Empirical EXAFS data analysis was performed with nonlinear least-squares curve-fitting techniques using empirical phase and amplitude parameters.[32,34−36] Empirical Fe−O and Fe−N backscattering parameters were obtained from $[Fe(acetylacetonate)_3]$[37,38] and $[Fe(1,10\text{-phenanthroline})_3](ClO_4)_3$[39,40] respectively. Fourier transforms (from k- to R-space) were performed for the data range of 3.5−14.5 Å^{-1} with a Gaussian window of 0.1 Å^{-1} to minimize truncation effects. The window widths used in the backtransforms (from R- to k-space) were 0.1 Å. The window widths were kept as similar as possible to those used to extract amplitude and phase parameters from the model compounds to minimize artifacts introduced by the Fourier filtering technique. All curve-fitting was done on k^3-weighted data and applied to the individual filtered shell of interest. A "goodness of fit" (GOF) parameter, F, was calculated as $F = \{[k^3(\text{data} - \text{fit})]^2/(\text{number of points})\}^{1/2}$ for each fit.

Theoretical EXAFS signals $\chi(k)$ were calculated using *FEFF* (version 6) and fit to the Fourier filtered data using EXAFSPAK (Dr. G. N. George, SSRL). The structural parameters varied were R (the bond distance), σ^2 (the bond variance), and E_0 (the threshold (k = 0 point) shift in eV). The σ^2 is related to the Debye−Waller factor, which is a measure of the thermal vibration and static disorder of the absorber-

(27) Whittaker, J. W.; Lipscomb, J. D.; Kent, T. A.; Münck, E. *J. Biol. Chem.* **1984**, *259*, 4466−4475.
(28) Whittaker, J. W.; Orville, A. M.; Lipscomb, J. D. *Methods Enzymol.* **1990**, *188*, 82−88.
(29) Fujisawa, H.; Uyeda, M.; Kojima, Y.; Nozaki, M.; Hayaishi, O. *J. Biol. Chem.* **1972**, *247*, 4414−4421.
(30) Browett, W. R.; Fucaloro, A. F.; Morgan, T. V.; Stephens, P. J. *J. Am. Chem. Soc.* **1983**, *105*, 1868−1872.
(31) Campochiaro, C.; Pavel, E. G.; Solomon, E. I. *Inorg. Chem.* **1995**, *34*, 4469−4675.
(32) Scott, R. A.; Hahn, J. E.; Doniach, S.; Freeman, H. C.; Hodgson, K. O. *J. Am. Chem. Soc.* **1982**, *104*, 5364−5369.
(33) Cramer, S. P.; Tench, O.; Yocum, M.; George, G. N. *Nucl. Instrum. Methods Phys. Res.* **1988**, *A266*, 586−591.
(34) Cramer, S. P.; Hodgson, K. O.; Stiefel, E. I.; Newton, W. E. *J. Am. Chem. Soc.* **1978**, *100*, 2748−2761.
(35) Cramer, S. P.; Hodgson, K. O. *Prog. Inorg. Chem.* **1979**, *25*, 1−39.
(36) Scott, R. A. *Methods Enzymol.* **1985**, *117*, 414−459.
(37) Iball, J.; Morgan, C. H. *Acta Crystallogr.* **1967**, *23*, 239−244.
(38) Roof, R. B. J. *Acta Crystallogr.* **1967**, *9*, 781−786.
(39) Johansson, L. *Chem Scr.* **1976**, *9*, 30−35.
(40) The crystal structure of the perchlorate salt has not been determined, but the $[Fe(phenanthroline)_3]^{2+}$ complex structure can be assumed to be identical to that of the corresponding iodide salt (Johansson, L.; Molund, M.; Oskarsson, Å. *Inorg. Chim. Acta* **1978**, *31*, 117).

scatterer pair. Although the threshold energy E_0 was allowed to vary in each fit, it was restricted to a common value for every component in that given fit. Coordination numbers were systematically varied in the course of the analysis, but were not allowed to vary within a given fit. Fits were evaluated by comparing the normalized error for the fits, calculated as the sum of the squares of the differences between experimental and calculated curves divided by the number of points. Bond valence sum analysis was performed in parallel with these fits to aid in evaluating the quality of a fit.

The intensities and energies of the pre-edge features of the protein data were quantitated with the fitting program EDG_FIT, (Dr. G. N. George, SSRL) which utilizes the double precision version of the public domain MINPAK fitting library. All spectra were fit over the range of 7108−7118 eV. Pre-edge features were modeled by pseudo-Voigt line shapes (simple sums of Lorentzian and Gaussian functions). A fixed 50:50 ratio of Lorentzian:Gaussian contributions for the pre-edge features successfully reproduced the spectra. Functions modeling the background contributions to the pre-edge features were chosen empirically to give the best fit and included pseudo-Voigt functions that mimicked shoulders on the rising edge. A fit was considered acceptable only if it successfully reproduced the data and the second derivative of the data. For all complexes, 8−10 fits were obtained which equally well reproduced the data and the second derivative with variation in the background function used. The value reported for the area of the fitted pre-edge, where peak area is approximated by the height multiplied by the full-width-at-half-maximum, is the average of all the pseudo-Voigt functions which successfully fitted the feature and its second derivative. To quantitate the error, the standard deviations for the peak energies and intensities were calculated from all of the pseudo-Voigt functions that fit the pre-edge features from all of the successful fits for each sample.

Results and Analysis

Circular Dichroism and Magnetic Circular Dichroism Spectroscopy. Near-IR CD at 4 °C and low-temperature MCD spectra (Figures 1A and 1B, respectively, solid line) were measured for dithionite-reduced high-spin ferrous 3,4-PCD. CD spectra taken with and without glycerol present and with and without the excess of dithionite removed were found to be unchanged. The Gaussian resolution of the data (dashed line in Figures 1A and 1B) indicates that there are two bands present, at 8075 and 10 400 cm^{-1} in the CD, and at 8433 and 10 466 cm^{-1} in the MCD. Comparison of the CD and MCD data indicates that there is a small temperature effect on the iron site that causes a minor decrease in the energy splitting in the MCD spectrum.

Distorted octahedral model complexes with biologically relevant oxygen and nitrogen ligation have two ligand field bands centered at ~10 000 cm^{-1} and split by <1800 cm^{-1}. In contrast, five-coordinate sites show one band at ~5000 cm^{-1} and a second at >10 000 cm^{-1} for square pyramidal structures which shift to lower energy for a trigonal bipyramidal geometry. Four-coordinate distorted tetrahedral sites only exhibit transitions in the 5000−7000 cm^{-1} region. From ligand field theory and by comparison to these model complexes, the observed MCD splitting (Δ^5E_g = 2033 cm^{-1}) and the energies of these two d→d transitions of reduced 3,4-PCD are consistent with a distorted octahedral six-coordinate active site.[23,24] The transition energies are most similar to those of the hexaquo weak ligand field models, $[Fe(H_2O)_6](SiF_6)$ and $[Fe(H_2O)_6](NH_4)_2(SO_4)_2$, which have absorption transitions at 8400 and 10 800 cm^{-1}, and 8700 and 10 300 cm^{-1}, respectively.[23] For $S = 2$ ground states, the inverse relationship between MCD intensity and temperature shown in Figure 1C is characteristic of *C*-term behavior in the negative ZFS case or to a temperature-dependent *B*-term intensity mechanism in the positive ZFS case and can be explored by VTVH MCD spectroscopy.[24,31]

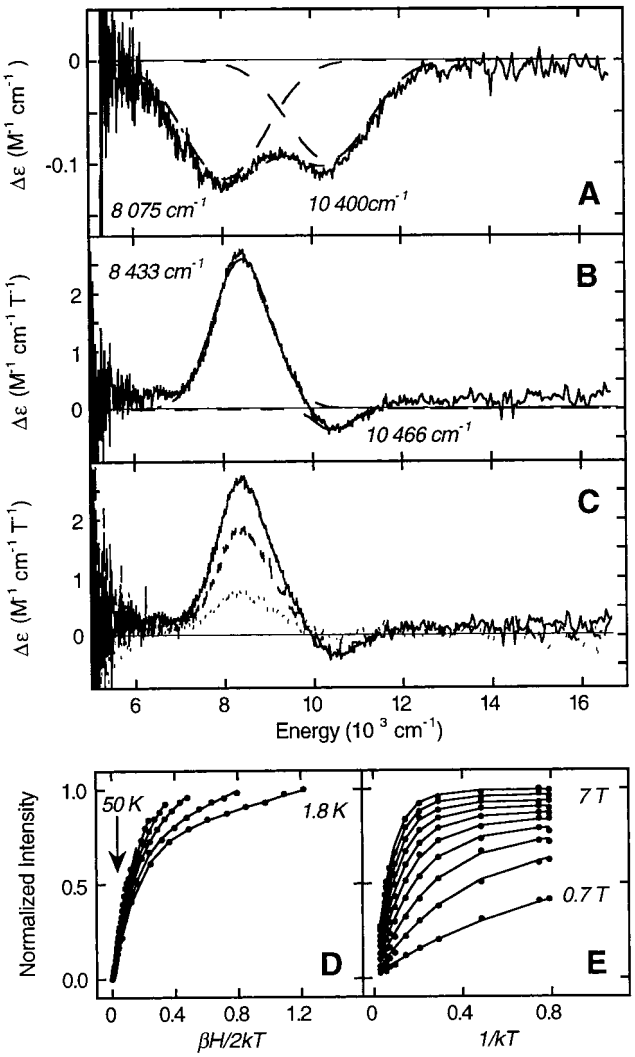

Figure 1. A. CD spectrum at 278 K of reduced 3,4-PCD (—), and the Gaussian fit (- - -) of the data. B. MCD spectra at 5 K and 7 T of reduced 3,4-PCD (—) and the Gaussian fit (- - -) of the data. C. Temperature dependence of the 7 T MCD spectra of reduced 3,4-PCD at 1.6 K (—), 15 K (— — —), and 50 K (- - -). D. VTVH saturation magnetization behavior recorded at 8245 cm^{-1} for reduced 3,4-PCD. The normalized data (•) and fit (—) of the data are plotted vs $\beta H/2k_BT$ for a series of fixed temperatures (1.8, 3.0, 4.9, 6.9, 10.0, 15.1, 20.2, 30.0, and 50.2 K; 1.9 K omitted for clarity). The standard deviations in the data points are approximately the size of the symbol used and have been omitted for clarity. E. The VTVH MCD data (•) and fit (—) replotted as a function of $1/k_BT$ for a series of fixed fields (0.7, 1.4, 2.1, 2.8, 3.5, 4.2, 4.9, 5.6, 6.3, and 7.0 T; 0.35 T omitted for clarity).

Variable-Temperature, Variable-Field Magnetic Circular Dichroism Spectroscopy. VTVH MCD data were collected at both 8245 and 10 417 cm^{-1} for a variety of temperatures and fields. The data for the transition at 8245 cm^{-1} (same as the data for 10 417 cm^{-1} but not shown) were normalized and plotted both as a function of $\beta H/2k_BT$ (Figure 1D) and $1/k_BT$ (Figure 1E) to separate the effects of temperature and field. By fitting the data to both positive and negative zero-field splitting (ZFS) models, the nested saturation magnetization isotherms (Figure 1D) were found to be best described by a negative ZFS non-Kramers doublet model. The decreasing spacing between curves of equal field increments in the low-temperature region of the $1/k_BT$ plot in Figure 1E is attributed to the rhombic splitting and mixing of the ±2 non-Kramers doublet wave functions.[24] The best fits to the data showed that reduced

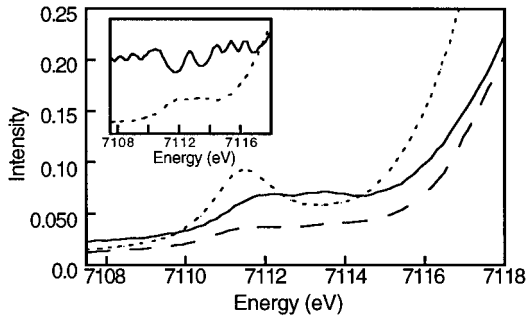

Figure 2. XAS pre-edge spectra of reduced 3,4-PCD (—) and the two model complexes $[Fe(TMC)CH_3CN]^{1+}$ (- - -) and $Fe(Im)_6^{2+}$ (— — —). The 3,4-PCD data (— — —) and the second derivative of the data (—) are depicted in the insert.

3,4-PCD has $\delta = 1.6 \pm 0.3$ cm^{-1}, and an excited singlet sublevel energy of ~24 cm^{-1}. Due to the interdependence of $g_{||}$ and a moderate *B*-term contribution that is also present, a unique value for $g_{||}$ could not be obtained for this system. For six-coordinate species, which are generally near the rhombic limit, δ typically is greater than 4 cm^{-1}, which corresponds to a small splitting of the $^5T_{2g}$ ground state, Δ (<500 cm^{-1}). The few exceptions where δ is less than 4 cm^{-1} have been attributed either to a rhombic site with one strong ligand−iron(II) π-bond leading to a large value of Δ,[23] or to a site close to the axial limit which corresponds to a small value of Δ.[41] Mössbauer data on the reduced 3,4-PCD site indicated a close to rhombic system with $|E/D| = 0.25 \pm 0.05$;[22] therefore, the small relative value of δ likely corresponds to a large value of Δ (~1500 cm^{-1}), the splitting to the $^5T_{2g}$ ground state, indicating a strong ligand−iron(II) π-bonding interaction (see ref 24 for details). From the oxidized 3,4-PCD ligand set, this will have to involve π-donor interactions of the tyrosinate ligand with the Fe(II) (vide infra).

X-ray Absorption Spectroscopy: Pre-edge. The pre-edge feature of dithionite-reduced 3,4-PCD is shown in Figure 2 together with that of $[Fe(Im)_6]^{2+}$ and $[Fe(TMC)CH_3CN]^{1+}$.[26] The second derivative of reduced 3,4-PCD (Figure 2 inset) clearly indicates two absorption transitions. Pseudo-Voigt fitting of the pre-edge feature, as described above, gives two transitions at 7111.8 and 7113.4 eV with areas of 5.7 and 3.0 units, respectively (Table 1).

Model studies have shown pre-edge shape and intensity patterns can be related to coordination number and geometry.[26] Six-coordinate ferrous complexes have a total pre-edge intensity of ~3.8 with a pre-edge shape that is broad and flat, where the lower energy feature is comprised of transitions to the $^4T_1$ and $^4T_2$ states, and the higher energy feature contains the transition into the higher lying $^4T_1$ d^7 parent state. In contrast, five- and four-coordinate ferrous models typically have two bands with a higher total pre-edge intensity of ~12.8. Furthermore, the intensity ratio of the low to high energy bands increase from six- to five- to four-coordinate complexes. The pre-edge of reduced 3,4-PCD is very similar in shape and intensity pattern to that of $[Fe(Im)_6]^{2+}$, a six-coordinate high-spin ferrous model complex. The total pre-edge intensity of 8.8 units for reduced 3,4-PCD is lower than that observed for four- and five-coordinate models (~12.8) but higher than that observed for six-coordinate models (~4.7).[26] The increase in intensity relative to six-coordinate models is associated with the overall loss of site symmetry in the protein relative to the model complexes. Fe(II) sites in proteins have been generally found to have higher intensities than model complexes.[42,43] Variations in bond lengths and mixed O/N ligation result in additional 4p mixing into the 3d orbitals; since the 1s→4p transition is dipole allowed, even a small amount of distortion can lead to a large increase in intensity.

X-ray Absorption Spectroscopy: EXAFS. EXAFS data on ferrous 3,4-PCD were measured to k of 15 Å^{-1} concurrently with the XAS edge data. The ferrous 3,4-PCD data show higher frequency oscillations than that of the oxidized form of the protein (Figure 3A), indicative of an overall increase in average bond length. The Fourier transform of the ferrous data over the range $k = 3.0-14.5$ Å^{-1} (Figure 3B) clearly shows a split first coordination sphere and three higher R peaks, possibly due to multiple scattering from tyrosine and histidine ligands. Both empirical and theoretical EXAFS fits were done on back-transformed ferrous 3,4-PCD data over the range $k = 3.5-14.0$ Å^{-1}. Since the results were virtually identical, only the theoretical results are discussed here.

Theoretical fitting of the Fourier-filtered EXAFS data from 1.1 to 2.5 Å confirmed that the first coordination sphere consists of multiple components. Although the use of only two components reasonably fits the ferrous 3,4-PCD data (fits 1 and 2 in Table 2), the reduced error is decreased by a factor of at least two by the addition of a third component. Several three component fits (fits 3−9 in Table 2) successfully reproduced the filtered EXAFS data retaining reasonable Debye−Waller factors. Of these, however, fits 3−6 have a significantly reduced error relative to fits 7−9 and only fits 3−6 have reasonable BVS values for ferrous systems, where the bond valence sum should be 2.00 ± 0.25 units.[44,45] While fits 3 and 4 are reasonable fits to the EXAFS data, they describe a five-coordinate site. Fits 5 and 6, however, have ligation distances of 1.91 (±0.02) Å, 2.08 (±0.02) Å, and 2.42 Å, and a total coordination number of six, which is consistent with the pre-edge and MCD analyses (vide supra). The fit to the filtered EXAFS data for ferric 3,4-PCD, with ligation distances of 1.88 and 2.10 Å, is provided for comparison (fit 10 in Table 2), and is very similar to that reported previously.[46] Two components adequately fit the ferric 3,4-PCD first coordination sphere and the addition of a third shell does not significantly improve the fit.

Discussion

From the ligand-field excited-state splitting of the ^5E_g orbitals (2033 cm^{-1}) obtained from CD and MCD spectroscopy and the XAS pre-edge intensity distribution and splitting pattern, the above studies have shown that upon reduction the active site of 3,4-PCD increases its coordination number from five to six. From the VTVH MCD analysis, a small value of δ was obtained, indicating a large value of Δ. This is unusual for a six-coordinate high-spin Fe(II) site and indicates the presence of a reasonably strong π-donor bond (vide infra). EXAFS spectroscopy indicates longer overall bond lengths in the ferrous site compared with the ferric enzyme, as expected upon reduction from a comparison to Fe(II) model complexes, with a BVS analysis of the distances also supporting a six-coordinate

(41) Kemsley, J. N.; Mitic, N.; Loeb Zaleski, K.; Caradonna, J. P.; Solomon, E. I. *J. Am. Chem. Soc.* **1998**, *121*, 1528−1536.
(42) Loeb, K. E.; Westre, T. E.; Kappock, T. J.; Mitic, N.; Glasfeld, E.; Caradonna, J. P.; Hedman, B.; Hodgson, K. O.; Solomon, E. I. *J. Am. Chem. Soc.* **1997**, *119*, 1901−1915.
(43) Pavlosky, M. A.; Zhang, Y.; Westre, T. E.; Gan, Q.-F.; Pavel, E. G.; Campochiaro, C.; Hedman, B.; Hodgson, K. O.; Solomon, E. I. *J. Am. Chem. Soc.* **1995**, *117*, 4316−4327.
(44) Brown, I. D.; Altermatt, D. *Acta Crystallogr.* **1985**, *B41*, 244−247.
(45) Thorpe, H. H. *Inorg. Chem.* **1992**, *31*, 1585−1588.
(46) True, A. E.; Orville, A. M.; Pearce, L. L.; Lipscomb, J. D.; Que, L., Jr. *Biochemistry* **1990**, *29*, 10847−10854.

Table 1. XAS Pre-edge Energies and Areas for Six-, Five-, and Four-Coordinate High-Spin Ferrous Model Complexes, and Oxidized and Reduced 3,4-PCD

compound	energy[a] (eV)	areas[a]	energy[a] (eV)	areas[a]	total area[a,b]
$[Fe(Im)_6]^{2+}$	7111.45 (0.04)	2.8 (0.1)	7113.36 (0.02)	1.9 (0.9)	4.7 (0.9)
$[Fe(TMC)CH_3CN]^{1+}$	7111.52 (0.04)	10.5 (0.8)	7113.30 (0.12)	2.2 (1.2)	12.7 (0.5)
$(Et_4N)_2[FeCl_4]$	7111.60 (0.02)	8.6 (0.4)	7113.12 (0.02)	4.3 (0.7)	12.9 (0.6)
Fe(III)PCD	7113.35 (0.02)	16.4 (1.7)	–	–	16.4 (1.7)
Fe(II)PCD	7111.81 (0.02)	5.7 (0.8)	7113.43 (0.03)	3.0 (0.4)	8.8 (0.9)

[a] The estimated standard deviations are reported in parentheses and were calculated as described in ref 26. [b] Variations where the sum of the individual peak areas do not equal the indicated total area due to round-off error.

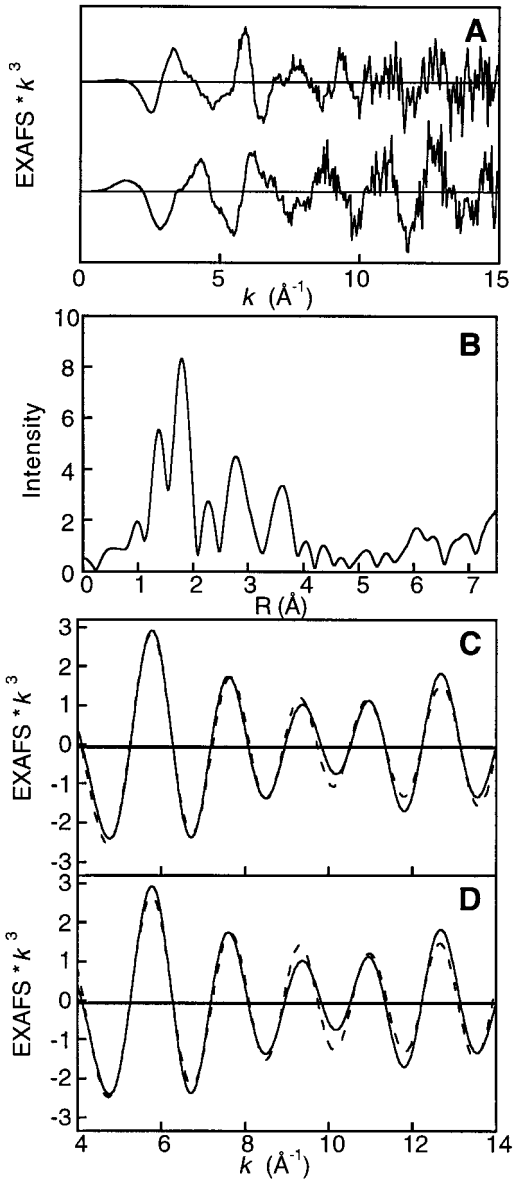

Figure 3. A. EXAFS spectrum of reduced 3,4-PCD (top) and oxidized 3,4-PCD (bottom). B. Nonphase shift corrected Fourier transform of the EXAFS data of reduced 3,4-PCD. C. Fit 5 (- - -) and data (—). D. Fit 6 (- - -) and data (—).

ferrous site.[47] A new long shell at 2.42 Å, that is not required to fit the ferric EXAFS data, is required for the reduced site, consistent with a new weak interaction.

X-ray crystallographic studies of the ferric active site of 3,4-PCD identified two histidines, two tyrosines and a hydroxide as the five active site ligands.[10] All spectroscopic studies conducted to date indicate that the iron ligand structure and active site environment of the 3,4-PCDs isolated from *P. putida* and *B. fuscum* are nearly identical.[1,2,9,13,15,27,46] The enzyme from *B. fuscum* has been used for all recent spectroscopic studies because the spectra are somewhat better resolved, indicating that the metal ligand environment is more homogeneous. Recently, the enzyme from *B. fuscum* has been crystallized.[48] In accord with the spectroscopic studies, the preliminary structure of this enzyme shows that the iron ligands and immediate environment are the same as previously reported for 3,4-PCD from *P. putida*.[49] Consequently, the known structure can be used in the analysis of the spectroscopic data reported here for the *B. fuscum* enzyme. From a comparison of iron-ligand bond lengths from the crystal structure to those obtained from theoretical EXAFS, specific EXAFS bond lengths can be assigned. The 1.88 Å distance appears to be associated with

Table 2. Summary of *FEFF* EXAFS Curve-Fitting Results for Ferrous and Ferric 3,4-PCD[a]

sample	fit no.	CN[b] (oxygen)	σ^2	bond length (Å)[c]	av bond length (Å)	E_o	error[d]	BVS[e]
Fe(II)PCD	1	2	0.00421	1.90	2.01	−14.6	.267	2.39
		3	0.00318	2.08				
	2	3	0.00780	1.93	1.99	−14.9	.219	2.45
		2	0.00146	2.09				
	3	1	0.00086	1.89	2.10	−14.8	.067	2.00
		3	0.00375	2.07				
		1	0.00575	2.41				
	4	2	0.00441	1.92	2.08	−15.9	.065	2.11
		2	0.00119	2.08				
		1	0.00613	2.42				
	5	1	0.00086	1.89	2.16	−14.8	.038	2.14
		3	0.00360	2.07				
		2	0.01098	2.42				
	6	2	0.00439	1.93	2.15	−16.3	.041	2.20
		2	0.00115	2.09				
		2	0.01120	2.42				
	7	2	0.00433	1.90	2.07	−16.8	.118	2.57
		3	0.00340	2.07				
		1	0.00496	2.40				
	8	1	0.00119	1.87	2.08	−15.9	.122	2.45
		4	0.00624	2.06				
		1	0.00397	2.39				
	9	3	0.00752	1.93	2.06	−17.2	.102	2.60
		2	0.00158	2.09				
		1	0.00587	2.40				
Fe(III)PCD	10	3	0.00238	1.88	1.97	−2.8	.203	
		2	0.00262	2.10				

[a] All fits were done with oxygen ligation. [b] CN = coordination number. [c] Errors in distances (±0.02 Å) are estimated from the variance between EXAFS fitting results and values from models of crystallographically known structure. [d] Error = F/no. of data points, where $F = (\Sigma[(\chi_{obsd} - \chi_{calcd})^2 k^6])$. [e] BVS = $\Sigma[\exp(r_i - r_0)/0.37]$; $r_0(O) = 1.700$ Å, $r_0(N) = 1.769$ Å.

(47) See, R. F.; Kruse, R. A.; Strub, W. M. *Inorg. Chem.* **1998**, *37*, 5369−5375.

(48) Earhart, C. A.; Radhakrishnan, R.; Orville, A. M.; Lipscomb, J. D.; Ohlendorf, D. H. *J. Mol. Biol.* **1994**, *236*, 374−376.

(49) Burk, D. L.; Ohlendorf, D. H. University of Minnesota, Minneapolis, MN. Personal communication, 1999.

the two tyrosinate ligands and the bound hydroxide, while the 2.10 Å distance would correlate to the two histidine ligands. Upon reduction, the coordination number increases from five to six, the overall EXAFS bond lengths concomitantly increase to 1.91 (±0.02) Å and 2.08 (±0.02) Å, and there is an additional long bond at 2.42 Å.

The new sixth ligand at the ferrous site, identified in the MCD, CD, and pre-edge studies (vide supra), is likely to be a water molecule since the crystallography has shown several water molecules in the adjacent substrate-binding pocket [10] The only nearby residue capable of coordination, Tyr16, is prevented from reaching the iron by steric constraints in the enzyme structure. Additionally, the hydroxide ligand present in the ferric site would be expected to become protonated in the reduced form since the pK_a of H_2O bound to Fe(III) is ~3, while that to Fe(II) is ~9, and the two tyrosinates would contribute considerable negative charge to the Fe(II) center also disfavoring ionization.[50] Thus there are probably two water molecules bound to the ferrous 3,4-PCD active site. If the tyrosinates do not protonate the active site would remain charge neutral, as has been shown to be important in 3,4-PCD.[12−16] This would indicate, that upon binding to Fe(II), the pK_a of tyrosine is lowered by at least 4 units, similar to the pK_a change observed for H_2O bound to Fe(II). A proposed structure for the six-coordinate ferrous site, based on the above analysis and a correlation of the ferric and ferrous EXAFS results, is shown on the right side of Scheme 1.

From the Pauling principle of charge neutrality, the residual charge on the central atom in a complex is expected to be close to zero,[51] indicating that a metal should require less charge donation from its ligand set upon reduction. This would imply that the coordination number might remain the same or decrease upon reduction with a given ligand set. Here we see the opposite behavior: an increase in coordination number upon reduction. The ferric active site, however, has a hydroxide ligand that would be expected to protonate upon reduction because of the reduced inductive effect for water coordinated to high-spin Fe(II) and therefore the higher pK_a as discussed above. Therefore, while the reduced metal center should require less charge donation from the ligands, protonation of one of the ligands and the presence of an unusually long bond would make the donor set much weaker, and an additional water could help satisfy the charge neutrality requirement of the metal center.

In high-spin model ferrous complexes, imidazoles have average bond lengths of ~2.20 Å,[47] Fe−OAr bond lengths range from 1.93 to 1.96 Å,[52−54] and water molecules typically have ligand−metal bond lengths of ~2.12 Å.[47] While, there are two good EXAFS fits of the ferrous data, both fits require a long distance and a short distance. By a comparison to the model complexes and the ferric EXAFS results, the short distance of 1.91 (±0.02) Å in the ferrous 3,4-PCD EXAFS fits would therefore be attributed to bound tyrosinate. From crystallographic studies, equivalent ligands bind to ferric 3,4-PCD with significantly different bond lengths depending upon the charge of the ligand in the *trans* position. In particular, anionic ligands binding opposite the equatorial Tyr408 have especially long bond lengths.[11−13,16] Consequently, the long distance of 2.41 Å from the EXAFS fits may be due to the solvent molecule opposite Tyr408. This bond is expected to be lengthened further due to hydrogen bonding of the water molecule with Arg457, which is thought to stabilize the negative charge of the catecholic anion bound to the iron site in the substrate complex of the ferric enzyme.[11,13] The large value of Δ from the VTVH MCD, while unusual for a six-coordinate high-spin ferrous site, can be understood in terms of the distortion in the ligand environment of reduced 3,4-PCD. In particular, the Fe−OTyr bond is quite short with an associated long *trans* H_2O bond. This would enhance the π-donor interaction of the tyrosinate with the iron and increase the splitting of the t_{2g} set of d-orbitals.

The results presented here show that the iron center in the active site of 3,4-PCD compensates for a change in metal charge by altering the nature of its ligand sphere, by both increasing the coordination from five to six and by protonation of the bound hydroxide, thus retaining charge neutrality. Changes of this type may be very important for the function of this enzyme and other dioxygenases. Moreover, the specific changes that occur are probably very sensitive to the placement and charge on the metal ligands that are present, thus allowing nature to fine-tune the active site to best facilitate the desired catalysis. For example, in ferric 3,4-PCD the reaction appears to proceed by electrophilic attack on O_2 directly on the C4 position of the metal-bound dianionic substrate.[1,2,13] By providing two displaceable anionic ligands (Tyr447 and OH^-) the enzyme favors chelation of the dianionic form of the substrate. Moreover, since one of the substrate hydroxyl functions must bind opposite the anionic Tyr408 while the other binds opposite neutral His462, the substrate−iron bond lengths are asymmetric causing the C4 position to be more negatively charged than the C3 position, thereby directing the site of electrophilic attack. The presence of so many anionic ligands also establishes a low redox potential for the iron, maintaining the ferric state and preventing initial O_2 binding to the iron. This contrasts with the proposed mechanism for the ferrous extradiol dioxygenase enzymes where the reaction appears to proceed by nucleophilic attack of iron-bound superoxide on a relatively electropositive carbon of the substrate ring.[1,2,19,55] Like the Fe(III) dioxygenases, the Fe(II) site of the extradiol dioxygenases is five-coordinate with an open site in the iron ligation.[1,18,20,56] However, in this case, only a single anionic glutamate residue is present in the endogenous iron coordination set along with two histidines residues and two solvent molecules, one of which may be ionized to establish a neutral center. EXAFS studies of the extradiol dioxygenase site show that the substrate binds as a monoanionic chelate, displacing the solvent molecules, and thus maintaining the neutral charge of the iron center.[19] Deprotonation of only one of the two hydroxyl functions, which does not activate the ring sufficiently for direct electrophilic attack by O_2, combined with the presence of Fe(II) and an open coordination site promotes initial binding of oxygen to the iron. Because the open coordination site is opposite the anionic carboxylate, the shift of electron density from the iron to the oxygen to yield a nascent superoxide moiety may be promoted. From this complex, in which both substrate and O_2 are bound to the iron, a reaction involving nucleophilic attack of the superoxide on the most electropositive site of the substrate ring, leading to extradiol cleavage, is readily conceivable. Thus, the ability of the active sites of the intradiol dioxygenase, 3,4-PCD, and the extradiol

(50) Baes, C. F., Jr.; Mesmer, R. E. *The Hydrolysis of Cations*; Wiley: New York, 1984.
(51) Pauling, L. *Contribution to the Study of Molecular Structure*; Maison Desoer: Liege, 1947.
(52) Chiou, Y.-M.; Que, L., Jr. *Inorg. Chem.* **1995**, *34*, 3577−3578.
(53) Cini, B. *Inorg. Chim. Acta* **1983**, *73*, 147−152.
(54) Jameson, G. B.; March, F. C.; Robinson, W. T.; Koon, S. S. *J. Chem. Soc., Dalton Trans.* **1978**, 185−191.
(55) Arciero, D. M.; Lipscomb, J. D. *J. Biol. Chem.* **1986**, *261*, 2170−2178.
(56) Mabrouk, P. A.; Orville, A. M.; Lipscomb, J. D.; Solomon, E. I. *J. Am. Chem. Soc.* **1991**, *113*, 4053−4061.

dioxygenases to modify their ligation in response to changes in charge of the metal and/or the ligands, may be important in their ability to function and specificity.

In summary, we have found that upon reduction the intradiol dioxygenase, 3,4-PCD, increases its coordination number from five to six, and we suggest a model for the six-coordinate site involving protonation of one of the coordinated ligands leading to the binding of a sixth ligand. The reduced site of 3,4-PCD has a large value of Δ which for rhombic systems is indicative of a strong π-bonding interaction, and is attributed to a short Fe−OTyr bond coupled with a long water bond *trans* to it. This study provides a basis for comparing the extradiol to the intradiol dioxygenases at the same oxidation level. In accord with our mechanistic proposals for the dioxygenases, it is shown that charge compensation in a biological system is a powerful force in creating a specific ligand sphere. Potentially, this can be adapted by nature to establish an effective catalytic center, or to dynamically alter an active site during the catalytic cycle to accelerate and direct the reaction chemistry.

Acknowledgment. This research was supported by NIH Grant GM40392 (E.I.S.), NIH Grant GM24689 (J.D.L.), NIH Grant RR1209 (K.O.H.), and NSF Grant CHE94-23181 (K.O.H.). J.M.Z. thanks the Jane Coffin Childs Fund for Medical Research for a postdoctoral fellowship. SSRL is funded by the Department of Energy, Office of Basic Energy Sciences. The SSRL Biotechnology program is funded by the National Institutes of Health, National Center for Research Resources, Biomedical Technology Program and the Department of Energy, Office of Biological and Environmental Research. The computing facilities of the Department of Chemistry at Stanford University are supported in part by a grant form the National Science Foundation (CHE-9408185).

IC981464P